TISSUE ENGINEERING: Part C
Volume 21, Number 1, 2015

DOI: 10.1089/ten.tec.2014.0040

An Immunocompetent, Orthotopic Mouse Model of Epithelial Ovarian Cancer Utilizing Tissue Engineered Tumor Cell Sheets

Ayumi Arauchi, MD, PhD,[1] Chieh-Hsiang Yang,[2] Sungpil Cho, PhD,[2] Elke A. Jarboe, MD,[3] C. Matthew Peterson, MD,[4,5] You Han Bae, PhD,[5,6] Teruo Okano, PhD,[1,5] and Margit M. Janát-Amsbury, MD, PhD[2,5,6]

Despite the development of a myriad of anticancer drugs that appeared promising in preclinical ovarian cancer animal models, they failed to predict efficacy in clinical testing. To improve the accuracy of preclinical testing of efficacy and toxicity, including pharmacokinetic and pharmacodynamic evaluations, a novel animal model was developed and characterized. In this study, murine ID8 (epithelial ovarian cancer [EOC]) cells as injected cell suspensions (ICS) and as intact cultured monolayer cell sheets (CS) were injected or surgically grafted, respectively, into the left ovarian bursa of 6–8 week-old, female C57BL/6 black mice and evaluated at 8 and 12 weeks after engraftment. Tumor volumes at 8 weeks were as follows: $30.712 \pm 18.800\,mm^3$ versus $55.837 \pm 10.711\,mm^3$ for ICS and CS, respectively, $p = 0.0990$ ($n = 5$). At 12 weeks, tumor volumes were $128.129 \pm 44.018\,mm^3$ versus $283.953 \pm 71.676\,mm^3$ for ICS and CS, respectively, $p = 0.0112$ ($n = 5$). The ovarian weights at 8 and 12 weeks were 0.02138 ± 0.01038 g versus 0.04954 ± 0.00667 g for ICS and CS, respectively (8 weeks), $p = 0.00602$ ($n = 5$); and 0.10594 ± 0.03043 g versus 0.39264 ± 0.09271 g for ICS and CS, respectively (12 weeks), $p = 0.0008$ ($n = 5$). These results confirm a significant accelerated tumorigenesis in CS-derived tumors compared with ICS-derived tumors when measured by tumor volume/time and ovarian weight/time. Furthermore, the CS-derived tumors closely replicated the metastatic spread found in human EOC and histopathological identity with the primary tumor of origin.

Introduction

Epithelial ovarian cancer (EOC) mortality exceeds the combined total of all other gynecologic malignancies and is the eighth leading cause of cancer in women, the seventh leading cause of all cancer-related deaths, making it the most lethal gynecologic malignancy in developed countries. It is estimated that 225,500 diagnosed and 140,200 deaths worldwide in 2008 were attributable to EOC.[1] Despite advances in the chemotherapeutic management of ovarian cancer, this malignancy maintains an unacceptably high mortality rate attributed to the delayed diagnosis and the development of drug resistance in initially chemosensitive tumors.[2] Since ovarian cancer is initially highly sensitive to chemotherapy, the need to more accurately model disease progression and therapeutic response is critical to successfully increase clinical survival rates.

The most common EOC histological subtype, accounting for >50% of ovarian epithelial malignancies, is serous ovarian carcinoma.[3] Due to the lack of early detection tools, the vast majority of serous ovarian carcinomas (>80%) are diagnosed at a more advanced stage[4] (stages III–IV), where the 5-year survival rate remains only 9–34%.[5] Most of these (>50%) are classified as ''high-grade'' tumors based on their degree of nuclear atypia and high mitotic index.[6] High-grade serous ovarian carcinomas (HGSOC type II) are characterized from other subtypes both for their aggressive nature and because they may harbor unique genetic alterations, including TP53 and the DNA repair genes BRCA 1 and 2. In contrast, clear cell, endometrioid, low-grade serous, and mucinous ovarian carcinomas typically present as indolent low-grade neoplasms (type I tumors) with somatic mutations in genes such as KRAS, BRAF, ERBB2, PTEN, CTNNB1, and PIK3CA.[7]

[1]Institute of Advanced Biomedical Engineering and Science, Tokyo Women's Medical University, Tokyo, Japan.
[2]Division of Gynecologic Oncology, Department of Obstetrics and Gynecology, University of Utah, Salt Lake City, Utah.
[3]Department of Pathology, Associated Regional University Pathologists (ARUP) University of Utah, Salt Lake City, Utah.
[4]Division of Reproductive Endocrinology and Infertility, Department of Obstetrics and Gynecology, University of Utah, Salt Lake City, Utah.
[5]Center for Nanomedicine, Nano Institute of Utah, Salt Lake City, Utah.
[6]Department of Pharmaceutics and Pharmaceutical Chemistry, University of Utah, Salt Lake City, Utah.

The ideal ovarian cancer animal model should closely replicate human disease etiology, genetic characteristics, tumor heterogeneity, and mimic interactions with the host immune system and relevant microenvironments. Various reviews[8,9] described different techniques to establish animal cancer models. Early models used chemical carcinogens to induce tumorigenesis,[10–12] modeling later advanced with the viral introduction of oncogenes inducing spontaneous tumors.[13,14] Though these models may enable spontaneous tumorigenesis, genetically engineered cancer mouse models[15] are associated with extremely high cost and difficulty for scalable reproducibility. Xenograft models utilizing human cancer cell lines are predominantly used to establish tumors in immune-deficient (nude) mice, and they are frequently created by subcutaneous, nonorthotopic single-cell injections. Therefore, the tumor site lacks the appropriate microenvironment and immune system interactions deemed relevant for the development of human EOC.[16] Orthotopic tumor origination may reproduce a more characteristic, metastatic spread of disease as well as a therapeutic response. Alexander reviewed the problems and shortcomings of current animal cancer models,[17] pointing out that the architectural and cellular complexity of actual tumors, including innate vasculature, stromal and inflammatory components in a specific anatomic location, cannot be faithfully replicated in cell culture. Furthermore, the xenograft–tumor–host interactions in a subcutaneous microenvironment are quite different than those found in the actual tissue of origin, thereby impacting drug response and therefore treatment outcomes.

In this project, we exploit the feasibility of engineered cell sheet (CS) cultures[18] as a novel concept for orthotopic ovarian tumor tissue engraftment in mice. CS tissue engineering offers several advantages compared with the conventional injection of single-cell suspensions. Tumor cell delivery occurs in the form of an intact cell monolayer preserving all cell–cell junctions, receptors, and the relevant extracellular matrix (ECM). Commercial plastic cell culture dishes grafted with a thin layer of temperature-responsive poly(N-isopropylacrylamide) (PIPAAm) enable culture and recovery of intact CSs by simply reducing the temperature from 37°C to room temperature (20–25°C).[19–21] This technique avoids harsh enzymatic treatments damaging cells during their dissociation into suspensions. Noncancerous CS cultures adhere rapidly to numerous different host tissues,[22–25] and promote improved graft quality and survival compared with tissue derived from injected cell suspensions (ICS).[26] For example, transplanted hepatocyte CSs express significantly greater hepatocyte-specific proteins, and demonstrate increased drug metabolism compared with hepatocyte ICS.[22] In cardiac repair experiments using transplanted myoblast CS tissues, increased formation of neocapillaries with reduced fibrosis was seen when compared with tissues derived from myoblast ICS.[27] Additional reports also confirm that large central necrotic areas are present in ICS-derived tissue constructs, whereas CS constructs exhibit homogenous stratified tissues without areas of observable necrosis.[28] Standard operating procedures have been established for the processes involved in CS tissue engineering, which have already advanced to be used in a recent regenerative medicine clinical trial.[29,30] Therefore, this technique now offers standardized, reproducible, operator-independent protocols that are translatable from noncancerous to cancerous cells and potentially will serve as preclinical animal testing platforms more efficiently and reliably screening novel anticancer therapeutics.

This study describes the development and characterization of an engineered EOC-CS animal tumor model. While CS techniques have been established for the *in vitro* and *in vivo* reconstruction of various other noncancerous tissue types,[31–33] this research represents an original effort to design and construct a novel animal model of EOC using CS technology. Its utility will be evident by demonstrating adequate tumorigenesis, improved tumor–tissue integration, greater fidelity to human ovarian tumor physiology and histology, and functionality in an immune-competent animal.

Materials and Methods

Cell culture

Murine ovarian ID8 cancer cells, a kind gift from Dr. G. Coukos (University of Pennsylvania), were derived from C57BL/6 mouse ovarian surface epithelial cells[34]; maintained in culture complete medium, Dulbecco's modified Eagle's medium (Sigma Aldrich) supplemented with 4% fetal bovine serum (Denville Scientific), 1% penicillin and streptomycin (Sigma Aldrich), and 1% insulin–transferrin–selenium (Invitrogen) at 37°C; and incubated in a humidified atmosphere of 5% CO_2. When ID8 cell cultures reached subconfluency, they were treated with trypsin-EDTA and resuspended in phosphate-buffered saline (PBS) for both ICS injection and CS fabrication.

Preparation of ID8 CSs

Temperature-responsive polymer (PIPAAm)-grafted cell culture dishes were provided (UpCell™; CellSeed) and used as previously described.[19] Through slight ambient temperature reduction, these dishes change surface properties and release attached cells without use of conventional dispase or trypsin protocols. This permits ease of culture and subsequent reliable collection of intact CSs. ID8 cells harvested using traditional enzymatic trypsin treatment on conventional cell culture plastics (Falcon) were transferred and seeded into 35 mm-diameter temperature-responsive culture dishes (CellSeed) (2×10^6 cells per one dish) in a humidified incubator with 5% CO_2 at 37°C for 24 h. When cells reached confluency, culture dishes were placed inside a laminar flow hood at room temperature (20–23°C) for 5–10 min to enable cells to detach from the surface in the form of an intact CS layer. ID8 CSs for implantation were prepared with a diameter of 6 mm. ID8 CSs were sectioned in half using a scalpel (Grafco Feather Sterile Scalpels; Disposable #11). To ensure equivalency of cell numbers used in ICS and in CS, numbers of cells (1×10^6) were counted before injection/transplantation and reconfirmed for CS after trypsinization of a separate dish not used for transplantation. The CS was then siphoned using a 10 μL pipette for transfer from the culture dish to animal ovarian tumor sites that were surgically prepared as described next. The remaining part of ID8 CS was preserved in paraformaldehyde for additional histological analyses.

Animals

Six- to 8-week-old female C57BL/6 mice (Jackson Laboratories) were housed and treated under standard conditions in the Animal Facility of the Center for Comparative

Medicine at the University of Utah according to approved protocols and guidelines of the Institutional Animal Care and Use Committee (IACUC).

Tumor initiation by ID8 ICS

ICS of ID8 cells in PBS were prepared immediately before an injection into animal tumor sites. Animals were randomly divided into nine groups with $n = 3$–5 per group. All animals undergoing surgical procedures were weighed before anesthetic injections (intraperitoneal xylazine–ketamine, 0.1 mL/10 g body weight). Each animal was placed in prone position and a dorsal incision of ~ 1.5 cm in length, slightly to the left of the midline, was made. The dermis was separated from underlying tissues, and a smaller incision was made through the dorsal fascia flat muscle to access the abdominal peritoneum. The left kidney was identified, and the area immediately below the kidney was dissected to locate the left ovary, which was then externalized through the incision. The control group ($n = 3$) received only a sham surgical procedure (SSP) without any injections into the ovary, and a second control group ($n = 3$) received an injection of 10 μL PBS (control) with SSP into the left ovarian bursa. All other groups ($n = 5$) received an injection of 1×10^6 ID8 cells (10 μL cell suspension in PBS) into the left ovarian bursa. ICSs were directly injected into the ovarian bursa using a Hamilton syringe (30G needle). After cell inoculation, the ovary was placed back into its original position in the peritoneal cavity. The back wall and skin incisions were sutured separately using 4-0 sutures. Control groups were sacrificed at 14 weeks after the surgical procedure. ID8 ICS injected groups were sacrificed at 8 weeks ($n = 5$), 12 weeks ($n = 5$), and 14 weeks ($n = 5$), respectively.

Tumor initiation by ID8 CS transplantation

Animals were randomized into four groups for sacrifice at 1 week ($n = 4$; one animal was lost during anesthesia), 4 weeks ($n = 5$), 8 weeks ($n = 5$), and 12 weeks ($n = 5$). To receive ID8 CS transplantations, animals were identically anesthetized and then, identical surgical site procedures were followed as described for animals in the ID8 ICS groups. Ovarian stromal tissue was accessed with a 1–1.5 mm incision to place ID8 CS. One half of a CS containing 1×10^6 cells was transplanted into the mouse ovaries using a 10 μL pipette. After allowing the transplanted CS to attach to the host ovarian tissue for about 2–3 min, the bursal incision was sutured closed using 4-0 sutures (Fig. 1A).

Ovarian volume and weight

All animals were sacrificed in accordance with the University of Utah IACUC-approved protocols. Oophorectomies were performed immediately after sacrificing mice at predetermined time points. Volumes and weights of the ovaries were captured by digital scale and caliper. Removed ovaries were formalin fixed, paraffin embedded and histopathological procedures were performed on a representative section of both tumor and normal ovary at each time point (at ARUP Laboratories).

Location and number of metastases

The location and number of metastases was determined. Every metastatic lesion in each affected organ was added to reach a final count for each organ and surface area (i.e., peritoneal sidewall) by visual observation.

Histopathology

Hematoxylin–eosin (H&E) staining and immunostaining with antibodies for CD31, vascular endothelial growth factor (VEGF), fibroblast activation protein (FAP) (ab28244; Abcam), and matrix metalloproteinase-2 (MMP-2) (ab15102; Abcam) were performed on the ID8 CS before transplantation as well as on resected ICS- and CS-generated tumor tissues at each time point. Human FAP/seprase is a surface glycoprotein expressed on cancer-associated fibroblasts (CAFs) in the majority of epithelial cancers, including EOC. Since FAP overexpression in human tumor cells has been shown to promote tumor growth in animal models and relate to the function of MMP-2, we used anti-FAP antibody and anti-MMP-2 antibody to stain the resected tissues (CS-derived tumors at 1, 8, and 12 weeks and ICS-derived tumors at 8 and 12 weeks).

After a 24 h culture period, ID8 CS and resected tissues were fixed in 4% paraformaldehyde (Wako Pure Chemical) and routinely processed into paraffin-embedded sections. H&E staining was performed per conventional protocols. Formalin-fixed, paraffin-embedded tissue sections that were 4 μm in thickness were placed on positively charged slides and dried in air. After drying, slides were melted in a 60°C oven for 30 min before they were placed on an automated stainer (Ventana Medical Systems). Slides were deparaffinized with EZ Prep solution (Ventana Medical Systems) and pretreated with CC1 (cell conditioning 1) for 30 min (Ventana Medical Systems).

H&E staining was performed as per conventional protocols. Immunohistochemical staining for CD31 was performed on representative tumor sections at each time point, whereas VEGF staining was only performed on CS-derived tumor tissue at the 1-week time point (ARUP Laboratories).[35] Briefly, to evaluate microvessel density in tumor tissues, staining for CD31 and VEGF was performed. Each primary antibody (CD31/1:50, ab 28364, or VEGF/1:50, ab 28364; Abcam) was applied to the slides for 2 h at 37°C after treatment with secondary antibody (rabbit IgG; Sigma Aldrich). The detection of slides was performed on the Ventana XT automated system using the IView DAB detection kit, which is a streptavidin-HRP system, utilizing 3-3′ diaminobenzidine (DAB) as the chromogen. Slide counterstaining was performed with hematoxylin. Digital images were acquired through a digital camera that was equipped with a microscope (Olympus BH-2; Olympus America, Inc.). The percentage of CD31 staining area was analyzed using ImageJ 1.44o software (NIH), and a minimum of five high-power (400×) fields of view were evaluated for each tissue.

In staining for FAP and MMP-2, primary antibodies were 1/1000 and 1/200 dilution, respectively. Tissues were incubated overnight at 4°C followed by secondary antibody for 1 h at room temperature. Enzymatic staining for FAP and MMP-2 with the use of LSAB2 kit (Dako Cytomation) was applied according to the manufacturer-suggested protocol. The counterstaining of slides was performed with Hematoxylin. The intensity of positive immunostaining was graded as +++, ++, and + for strong, moderate, and weak results, respectively.

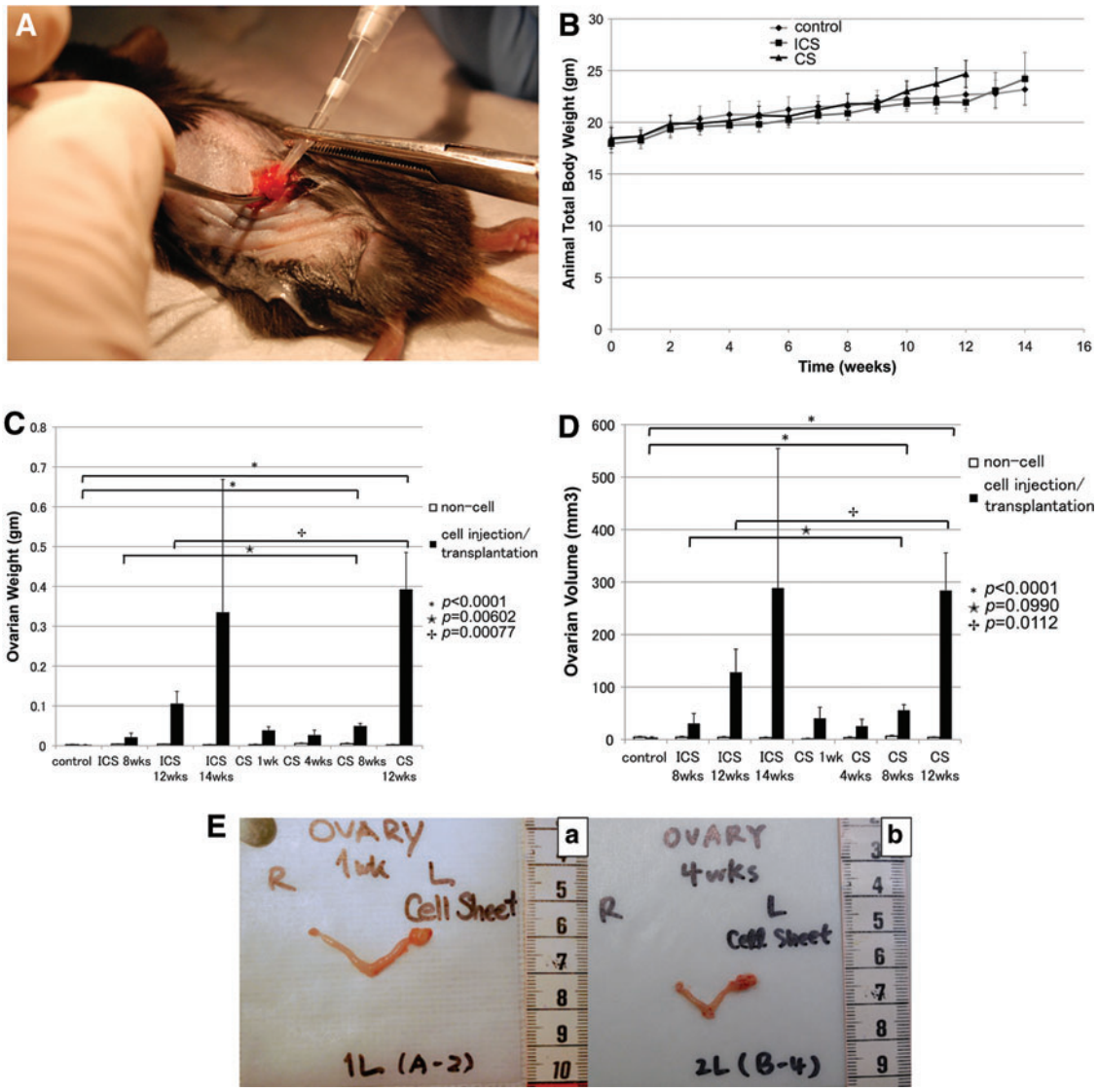

FIG. 1. **(A)** Surgical procedure: cell sheet (CS)-transplantation. To transplant ID8 CSs, microsurgery was used to place CSs directly underneath the ovarian bursa of 6–8 week-old, female C57BL/6 mice. **(B)** Total animal body weights. Body weights were recorded bi-weekly and immediately before surgeries. Both injected cell suspensions (ICS) and CS transplantation groups as well as control groups gradually gained weight over 10 weeks. At the 12 week time point, weight gain in the CS transplantation groups accelerated significantly compared with ICS and controls ($p=0.0081$, $p=0.1595$, respectively). **(C)** Ovarian weights. Ovaries were harvested at each time point, separated from uterine tubes, and weighed. On comparing controls and CS groups at 8 and 12 weeks, a significant difference was found ($p<0.0001$). Significant differences were seen in ICS versus CS groups at 8 weeks ($p=0.006$) and 12 weeks ($p=0.0008$). **(D)** Ovarian volume. Ovaries were harvested at each time point, separated from uterine tubes and ovarian volumes were determined according to $V=0.5\times(L\times W)^2$, with L being the tumor length (longest dimension) and W the width (shortest dimension). Both ovarian weights and volumes demonstrated significant differences at the 8 and 12 week time points ($p<0.0001$). Moreover, both ICS and CS groups presented with differences at 8 weeks ($p=0.0990$) and more obvious difference at 12 weeks ($p=0.0112$). **(E)** Bilateral hystero-oophorectomies were performed at predetermined time points. **(a)** One week post-transplantation of the ID8 CS. Weight: 0.00245 ± 0.001 g versus 0.03873 ± 0.009 g ($p<0.001$, $n=4$), volume: $1.459\pm0.71\,mm^3$ versus $40.35935\pm21.102\,mm^3$ ($p=0.035$, $n=4$) for noncancerous and cancerous ovaries, respectively. **(b)** Four weeks post-transplantation of the ID8 CS. Weight: 0.0058 ± 0.00076 g versus 0.02682 ± 0.012336 g ($p=0.014$, $n=5$), volume $3.6272\pm1.20696\,mm^3$ versus $25.5356\pm13.11968\,mm^3$ ($p=0.012$, $n=5$) for noncancerous and cancerous ovaries, respectively. Color images available online at www.liebertpub.com/tec

Statistical analysis

Values are expressed as mean ± standard deviation. Data were plotted using Excel, and statistical analyses were performed using ANOVA and Student's *t*-test analysis (using JMP® software version9).

Results

Comparison of ID8 ICS-derived tumors versus ID8 CS-derived tumors

Total body weight (TBW) was measured twice to thrice per week starting on day 1 postsurgery (Fig. 1B). TBW

increases were similar across all groups for the first 10 weeks. Starting at 10 weeks, TBW for the CS transplantation group (23 ± 1 g) was slightly greater than for the ICS injection group (21.82 ± 0.53 g). After reaching 12 weeks, a significant difference could be observed (24.68 ± 1.304 g versus 21.93 ± 0.65 g, ICS and CS, respectively; $p < 0.001$, $n = 5$). No significant difference was found between the ICS injection group and the CS transplantation group with regard to volume and weight of control ovaries (right side) not receiving any ID8 tumor cells (Fig. 1C, D).

Volume and weight of cancerous ovaries (left side) having received either ICS injections or CS transplantations significantly increased compared with contralateral, healthy ovaries (Fig. 1E). Ovarian weights of the CS-grafted groups were much higher than those of the control groups. The most significant increase in ovarian weight was noted after 8 weeks for the CS-transplanted groups (0.04954 ± 0.00667 g) when ovarian weights increased more than twofold compared with tumors within the ICS groups (0.02138 ± 0.01038 g) ($p = 0.00602$). Further, a significant difference was found when comparing the ovarian weights of ICS-injected groups (0.10594 ± 0.03043 g) with CS-transplanted groups (0.39264 ± 0.09271 g) after 12 weeks ($p = 0.00077$) (Fig. 1C). Furthermore, ovarian volume indirectly correlated to ovarian weight at the 8 weeks: $30.712 \pm 18.800\,mm^3$ for ICS versus $55.837 \pm 10.711\,mm^3$ for CS, $p = 0.0990$, and 12 week; $128.129 \pm 44.018\,mm^3$ for ICS compared with $283.953 \pm 71.676\,mm^3$ for CS, $p = 0.0112$) (Fig. 1D).

Metastases

On comparing the total numbers of metastases at the 8-week time point, animals with CS-derived tumors ($n = 42$) had developed twice as many metastases as animals with ICS-derived tumors ($n = 19$). The total metastatic count was only 150 for the five animals within the 12-week ICS group ($n = 161$) and >400 among all five animals within the 12-week CS group ($n = 405$) (Fig. 2A). On comparing the locations of metastases at the 8-week time point for animals in the ICS injection groups, metastatic dissemination was localized to visceral organs in close proximity of the ovary (i.e., kidney, fallopian with uterine tube, and spleen). After 12 weeks, lesions had spread further

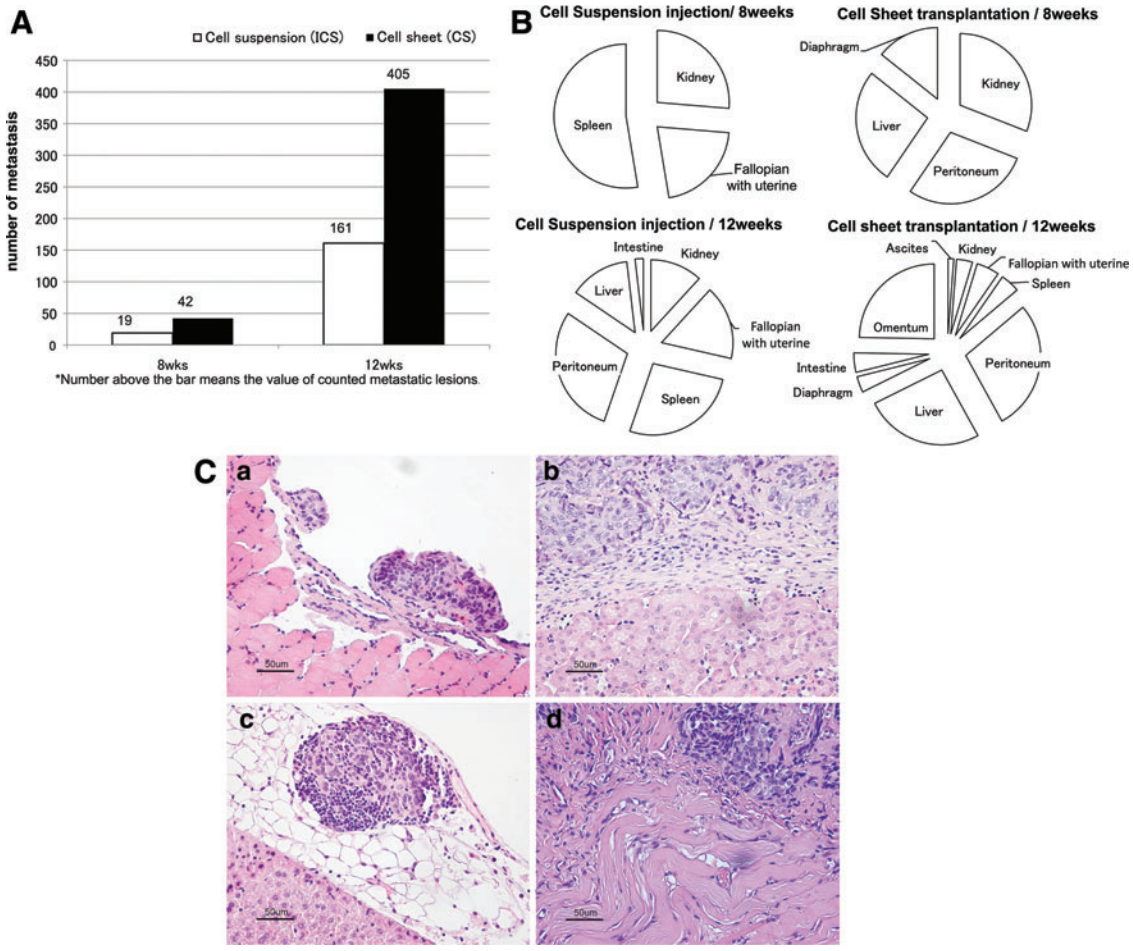

FIG. 2. **(A)** Metastatic count (N_M). Number of grossly visible metastases was counted without magnification. After 8 weeks, animals with CS-derived tumors had developed more metastases ($N_M = 42$) compared with animals with ICS-derived tumors ($N_M = 19$). The total metastatic count was >405 among animals ($n = 5$) in the 12-week CS group and 161 for animals ($n = 5$) within the 12-week ICS group. **(B)** Pattern of metastatic spread after 8 and 12 weeks. Metastatic progression based on the organs affected was analyzed on comparing the ICS versus CS transplantation groups after 8 and 12 weeks of tumor growth, respectively. **(C)** Metastases formed after 8 weeks in animals bearing ID8 CS-derived tumors. Scale bar is 50 μm ($\times 200$). **(a)** Diaphragm, **(b)** kidney, **(c)** liver, and **(d)** peritoneum. Color images available online at www.liebertpub.com/tec

across the peritoneal cavity, including the liver and intestines. In contrast, CS-transplanted groups exhibited metastases on the peritoneal sidewall, liver, kidney, and diaphragm by 8 weeks. In addition, by 12 weeks, ascites had also developed in these animals and metastases had spread to the fallopian with uterine tube, spleen, intestine, and omentum (Fig. 2B). In each case, the foci of the extraovarian tumor identified were morphologically identical to the primary ovarian tumor. Similar to the ovarian tumor, the extraovarian tumors were characterized by high-grade malignant cells with minimal cytoplasm and atypical nuclei, which were arranged in variably sized nests and poorly formed glands (Fig. 2C).

Morphological examination for ID8 CSs in vitro

Each engineered CS included 2×10^6 ID8 seeded cells per one temperature-responsive culture dish of 35 mm diameter size. Cell populations displayed no significant morphological changes within 24 h before seeding in culture. A histological examination of ID8 CS demonstrated that cells

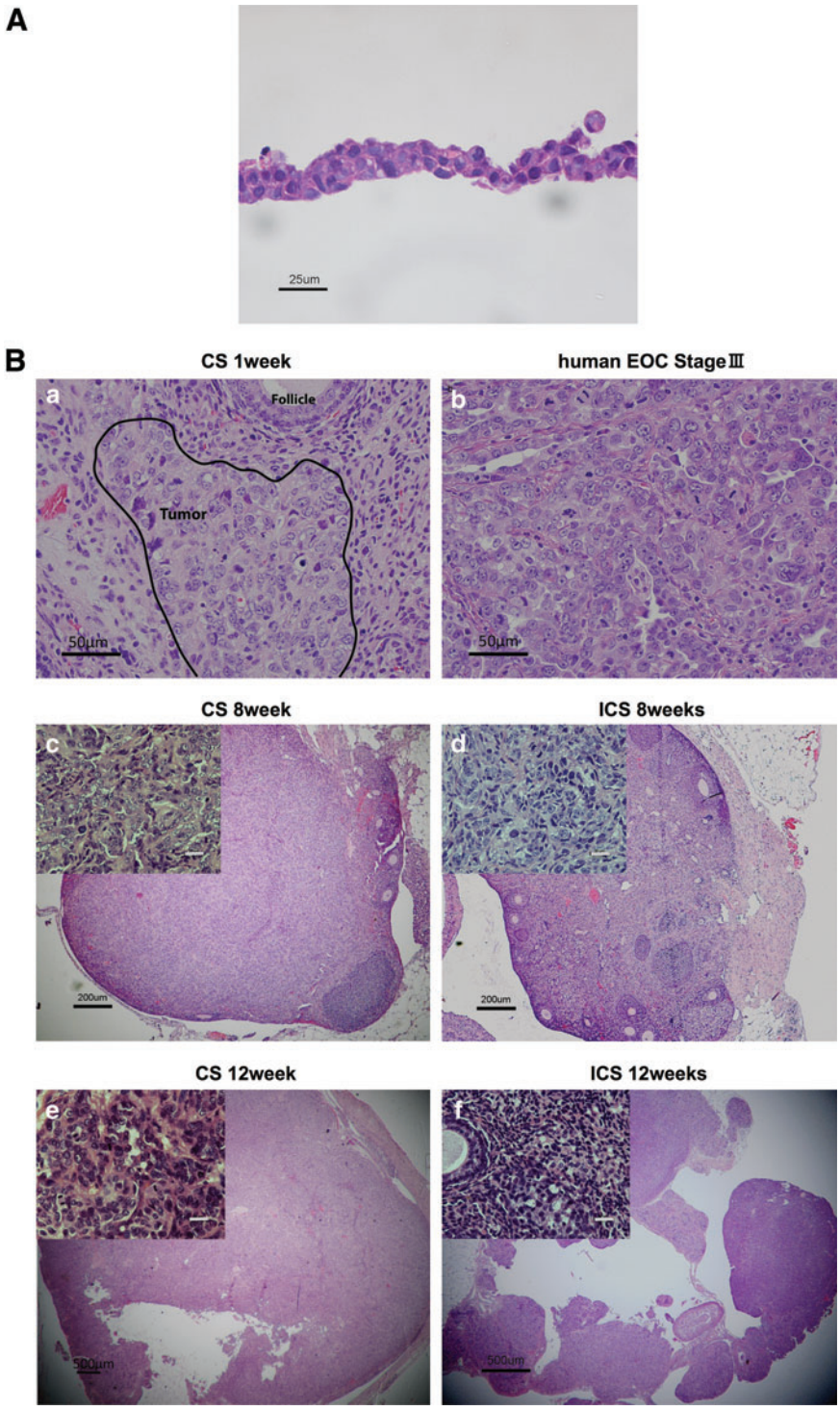

FIG. 3. **(A)** Histology of a cultured ID8 CS. Hematoxylin–eosin (H&E) stain for a representative ID8 monolayer CS. After 24 h of culturing, tight junctions were noted between cells. Cell morphology revealed an irregular cellular morphology with nuclear atypia. Scale bar is 25 μm (×400). **(B)** Murine CS-derived epithelial ovarian cancer (EOC) tumor versus human stage III EOC tumor. **(a)** H&E stain of a resected mouse ovary at 1 week after ID8 CS transplantation. Scale bar is 50 μm (×200). Cancerous infiltration of the CS into ovarian parenchyma could be identified (area inscribed with block line). Cell morphology resembled **(b)** human EOC, stage III (H&E). Scale bar is 50 μm (×200). **(c)** At 8 weeks post-transplantation, ID8 CS tumors had partially invaded the ovary and replaced original ovarian structure, whereas **(d)** ICS tumors were still confined to the ovarian bursa. Scale bar is 200 μm (×40), small window; scale bar is 20 μm (×400). Tumor volumes at 8 weeks were $30.712 \pm 18.800\,mm^3$ versus $55.837 \pm 10.711\,mm^3$ for ICS and CS, respectively, $p = 0.0990$ ($n = 5$). **(e)** Twelve weeks post-transplantation, the ID8 CS tumors occupied almost the entire ovary. Scale bar is 500 μm (×20), small window; scale bar is 20 μm (×400). **(f)** After 12 weeks of ICS tumor growth, the entire ovary showed malignant histology and tumor volumes were significantly larger ($283.953 \pm 71.676\,mm^3$) than ICS tumors ($128.129 \pm 44.018\,mm^3$), $p = 0.0112$ ($n = 5$). Scale bar is 500 μm (×20), small window; scale bar is 20 μm (×400). Color images available online at www.liebertpub.com/tec

showed irregular shapes and sizes, with scant cytoplasm, numerous mitotic figures, and nuclear atypia indicative of a typical malignancy (Fig. 3A).

Morphological comparison of in vivo *ID8 ICS-derived versus ID8 CS-derived tumors*

H&E staining confirmed ID8 cell-derived tumors in the ovarian bursa invading the ovary as early as 1 week after orthotopic CS transplantation. Transitional zones to normal, noncancerous tissues were clearly identifiable within the ovary (Fig. 3B-a) after 1 week with histological characteristics being similar to human spontaneous EOC (Fig. 3B-b). Furthermore, normal stromal tissue structure and histology in tumor were maintained and the ID8 cells displayed their typical characteristic features, including irregular shape and size of the cells, nuclear atypia, abnormal nuclear-cytoplasmatic ratios, and the presence of mitotic figures (Fig. 3B-a).

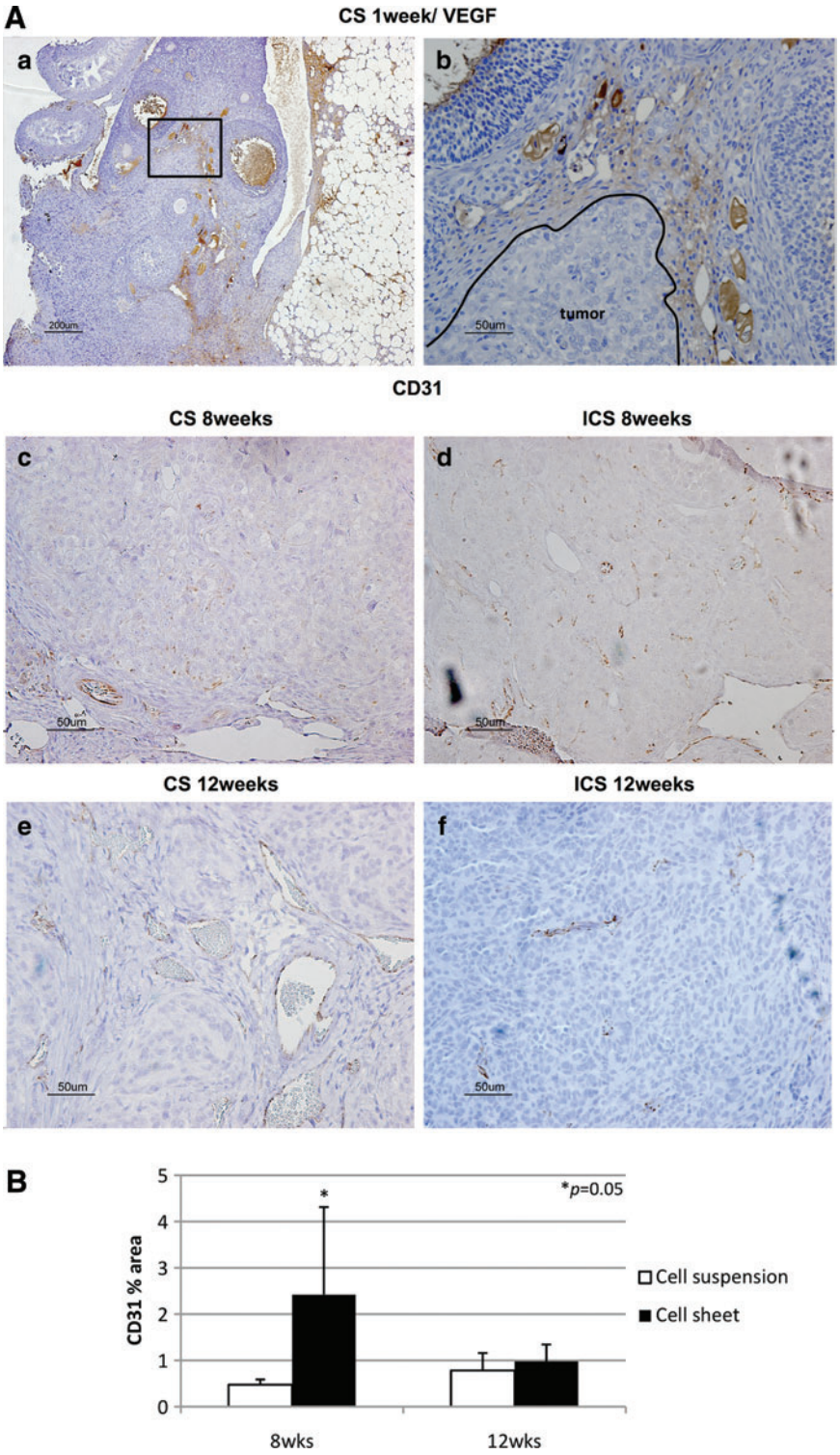

FIG. 4. **(A)** Vascular endothelial growth factor (VEGF) and CD31 immunostaining. **(a)** VEGF-positive margins were found surrounding CS-derived tumors at 1 week post-transplantation, ×40, scale bar is 200 μm and **(b)** was magnified from a small frame in **(a)**, ×200, scale bar is 50 μm. Based on immunohistochemical expression of CD31, microvessels were displayed more densely in the CS-derived than in ICS-derived tumors at 8 weeks **(c, d,** respectively). At 8 weeks, 0.475% ± 0.113% area versus 2.420% ± 1.893% area displayed positively in ICS-derived tumors and CS-derived tumors, respectively ($p = 0.05$). This finding intensified further after 12 weeks with ICS tumors exhibiting only 0.782% ± 0.378% area versus CS tumors exhibiting 0.979% ± 0.364% area ($p = 0.43$) **(e, f)**. Scale bar is 50 μm (×200). **(B)** Microvessel density. Percentage of CD31 positive-stained areas were compared using ImageJ 1.44o software (NIH). Images of CS-derived and ICS-derived tumors were compared and analyzed. At 8 weeks, CS-derived tumors exhibited 2.420% ± 1.893% area versus ICS-derived tumors only showing 0.475% ± 0.113% area positive for CD31 ($p = 0.05$). At 12 weeks, CS-derived tumors were 0.979% ± 0.364% area versus ICS-derived tumors were 0.782% ± 0.378% area ($p = 0.43$). Color images available online at www.liebertpub.com/tec

Moreover, nearly all of the original normal structure of the ovary was replaced by metastatic tumor features in the CS-derived tumors when compared with the ICS-induced tumors at 8 weeks (Fig. 3B-c, d). After 12 weeks, the entire ovary was replaced by a tumor with malignant histology, and the volumes of CS-initiated tumors were rapidly growing compared with the tumors formed in ICS-treated ovaries (Fig. 3B-e, f). Further, CS-initiated tumors grew invasively, infiltrating the ovarian parenchyma. VEGF immunostaining of CS-derived tumors harvested at 1 week post-transplantation was positive (Fig. 4A-a, b). Immunohistochemical expression of the angiogenetic factor, CD31 revealed that the area including microvasculature at 8 weeks was stained to $0.475\% \pm 0.113\%$ in ICS-derived tumors versus $2.420\% \pm 1.893\%$ area in CS-derived tumors ($p = 0.05$) (Fig. 4A-c, d, B). At 12 weeks, $0.782\% \pm 0.378\%$ area versus $0.979\% \pm 0.364\%$ area displayed positive CD31 staining in ICS-derived tumors and CS-derived tumors, respectively ($p = 0.43$) (Fig. 4A-e, f, B). Tissue staining for FAP showed overlapping expression with MMP-2 in stromal cells of both the ICS-derived and CS-derived tumors (Fig. 5). CS tumors stained positive for FAP and MMP-2 strongest (+++) within the stromal tissue at 1 week post-CS transplantation (Fig. 5a, b), then gradually decreased over time (8, 12 weeks; ++) (Fig. 5c–f). FAP and MMP-2 expression increased from 8 weeks (+) to 12 weeks (+++) in the ICS-derived tumor (Fig. 5g–j).

Discussion

In a previous study, we reported that ID8 tumorigenesis required ~60 days post-ICS injection.[35] A sentinel finding in this study was a significantly shortened tumorigenesis requiring only 7 days post-transplantation when utilizing the

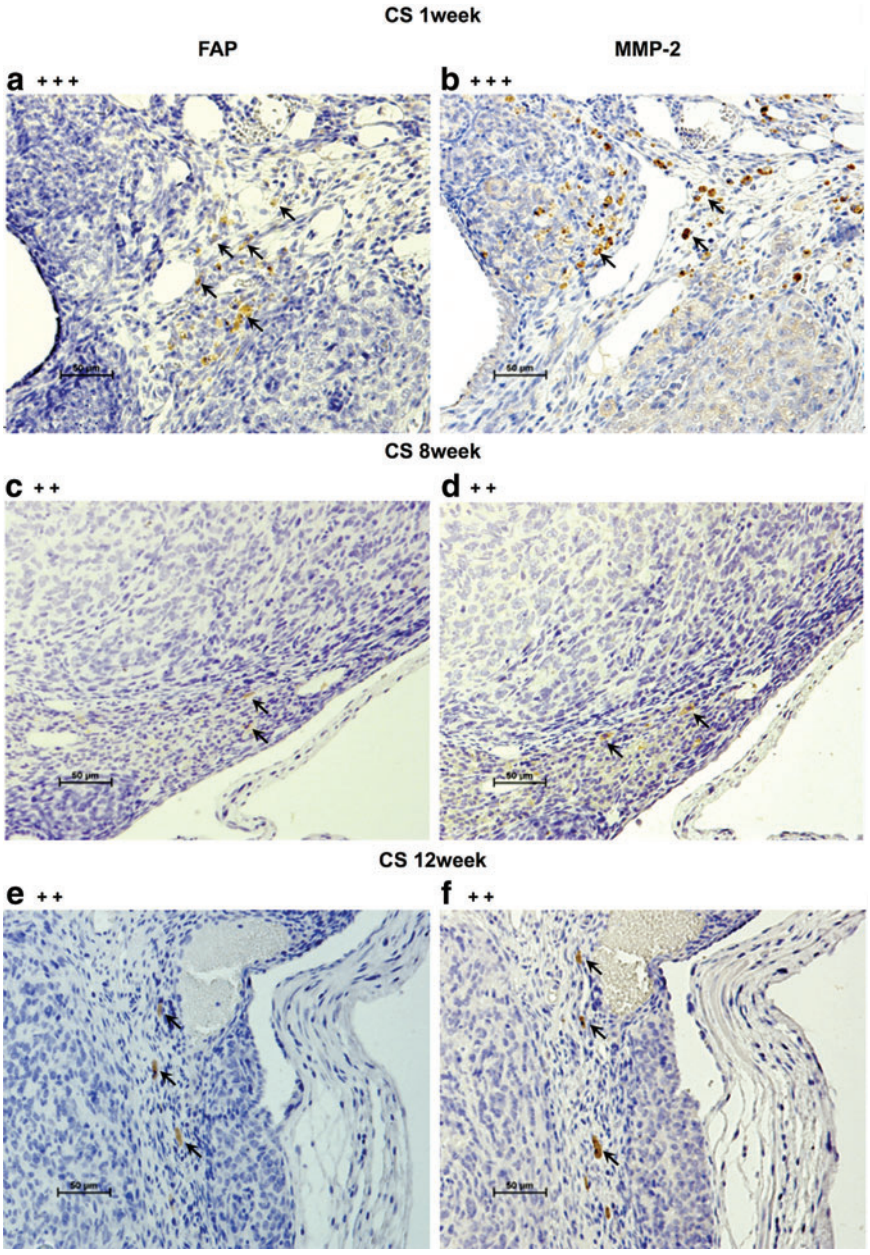

FIG. 5. Fibroblast activation protein (FAP) and matrix metalloproteinase-2 (MMP-2) expression. Scale bar is 50 μm (×200). **(a)** shows FAP-positive cells stained in brown (arrow) at 1 week in CS-derived tumor. **(b)** shows MMP-2-positive stroma stained in brown (arrow) at 1 week in CS-derived tumor. **(c, d)** show positive expression for FAP, MMP-2 at 8 weeks in CS-derived tumors (arrow). **(e, f)** show a decrease in FAP, MMP-2 after 12 weeks of CS-derived tumor growth (arrow). **(g, h)** show low FAP, MMP-2 expression at 8 weeks for ICS tumors (arrow). **(i, j)** show decreased FAP, MMP-2 expression after 12 weeks of ICS tumor growth. Color images available online at www.liebertpub.com/tec

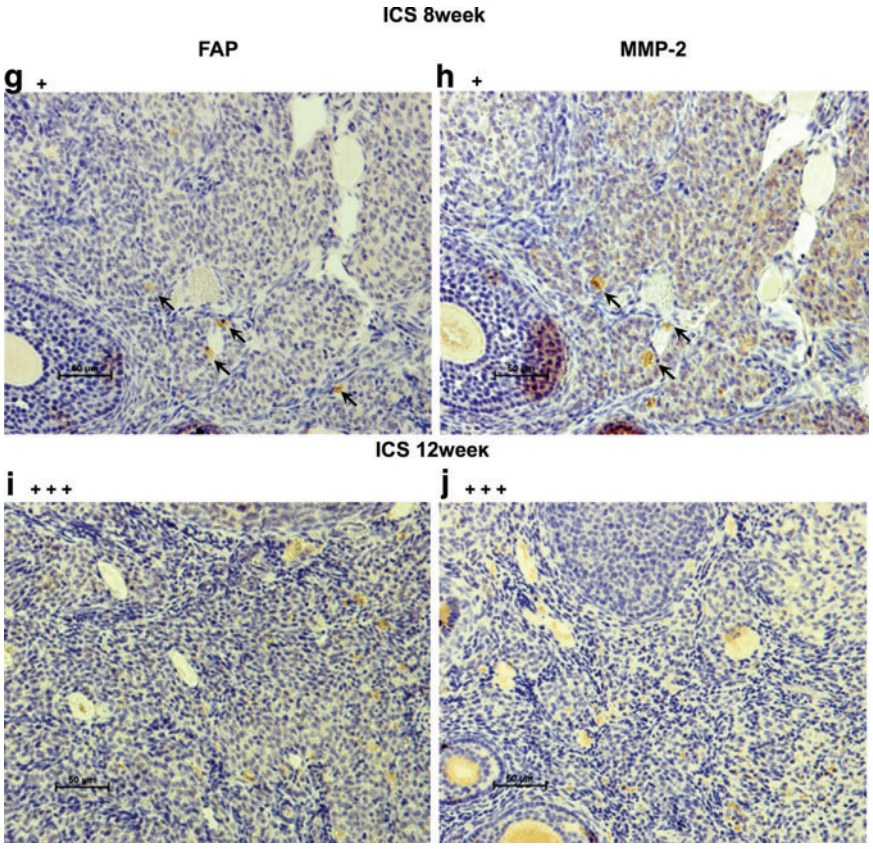

FIG. 5. (Continued).

CS approach in the same immune-competent animal model. This phenomenon may be due to the fact that CS technology retains cell–cell junctional complexes, expression of key membrane proteins and antigens, and the continued secretion of cytokines at the time of transplantation. Yamato *et al.* showed that E-cadherin and laminin-5 production, products of ECM, are maintained in the keratinocyte sheets harvested from temperature-responsive culture dishes.[36] The remarkably rapid ID8 CS fabrication within 24 h and significant reduction in time for *in vivo* tumor initiation, progression, invasion, and metastasis suggest that ECM deposition and expression of critical cancer inducing factors may be a key advantage provided by CS technology.

Generally, solid tumor consists of various other components besides cancer cells such as specific stroma, which is constructed from ECM, fibroblasts, inflammatory cells, and tumor-associated endothelial cells, cooperating to promote cancer cell propagation, survival, migration, invasion, and metastasis at tumor sites.[37] Due to the very limited space while manipulating CS with a 10 μL pipette, CSs were folded in some cases instead of being spread evenly as one single, flat layer onto the ovarian surface beneath the bursa. This modification led to inherent cell–cell interactions, including associated ECM, which were capable, despite folding, of maximizing cell retention and adherence within the bursal confines. Thus, the properties enhancing engraftment did not appear to be dependent on a single cell layer of CS adherence and were present despite marginal folding. This suggests that CS can be utilized in a variety of applications as tissue packets and not necessarily as a monolayer sheet.

The differentiation of ovarian carcinomas is very complex.[38] Tumors form polarized epithelia, papillae, cysts, and glandular structures. Morphological examination of ID8-CS *in vitro* displayed heterogeneity of various cell types, including both cancerous cells and fibroblast-like cells, very much akin to the findings in human EOC. Our *in vivo* experiments also showed similar morphological characteristics, including papillary tumor growth, multilayered epithelia, including stromal and capsular invasion (Fig. 6).

Noteworthy was the metastatic pattern in animals bearing orthotopically CS-transplanted tumors, which closely mimicked the metastatic spread in spontaneous human ovarian cancers. In general, serous ovarian cancer cells through surface shedding are disseminated within the peritoneal cavity carried by the peritoneal fluid to the peritoneum, diaphragm, and omentum.[39,40] Ipsilateral kidney metastases were noted after 8 weeks in animals bearing CS-derived tumors, This type of metastatic spread is indicative for local surface shedding. After 12 weeks, animals, in addition to forming multiple metastases in various locations, also developed ascites, which was associated with hepatic and omental metastases (responsible for the animals' body weight gain starting around 10 weeks).

According to numerous reports, CAFs appear to enhance cancer cell invasion and metastasis. CAFs promote the ECM deposition, resulting in cancer fibrosis, and also MMP secretion, which is effective for resolving ECM, plays an important role in tumor growth and invasion.[41] Multiple other studies used anti-FAP antibody as a useful marker to detect CAFs[42–44] in induced animal tumor models. Enhanced tumorigenesis of the CS-derived ovarian tumors

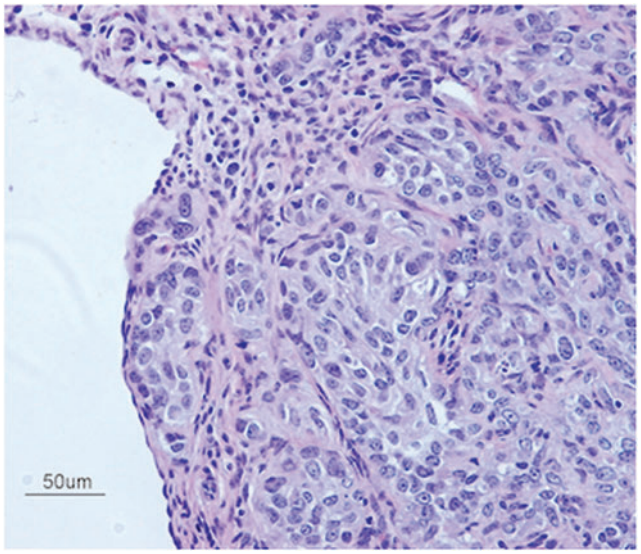

FIG. 6. H&E staining reveals malignant epithelioid cells arranged in variably sized nests within CS-derived tumor at 8 weeks post-transplantation. The cells themselves have a minimal to moderate amount of eosinophilic cytoplasm and atypical nuclei exhibiting anisonucleosis, coarse chromatin, and variably conspicuous nucleoli. Scattered mitotic figures are noted. Scale bar is 50 μm (×200). Color images available online at www.liebertpub.com/tec

may have been, in part, promoted by the natural orthotopic microenvironment, which provided FAP-expressing fibroblasts that potentially were induced by CS graft ECM factors.

MMP-2 immunostaining demonstrated a significant expression within the stroma of CS-derived tumors during the first week of tumorigenesis, compared with ICS-induced tumors. Torng *et al.* reported that stromal MMP-2, indeed, occurs early and may play a role in early EOC invasion having a key role in matrix remodeling by fibroblasts.[45] Furthermore, an association between MMP-2 and the invasion and metastasis of ovarian cancer has already been reported.[46] It is known that both force-mediated and protease-mediated matrix remodeling play a role in tumor invasion, and it has been reported that fibroblasts actively generate tracks through the neighboring stroma of tumor cells.[41] Our findings confirmed the expression of FAP and MMP-2 not only within the stroma surrounding the tumor but also in tissues not immediately adjacent to the tumor. This suggests that stromal fibroblasts may release MMP-2 and may also play a role in invasion and stromal remodeling, which is critical to initiate tumor invasion and cell migration. It appears that the ID8 CS-derived ovarian cancer model described here replicates the MMP-2-associated pattern of tumor invasion in the ovary.

Mesothelial cells covering organs located within the peritoneal cavity are purported to be the first line of defense to inhibit ovarian cancer cell adhesion and invasion.[47,48] CS-derived, orthotopic, immunocompetent models of EOC could potentially offer a feasible new model that more closely replicates the human scenario. Mesothelial cells stimulate the migration of white blood cells in response to inflammatory mediators. After coculturing primary human mesothelial and ovarian cancer cells, both of which are extracted from ascites on ECM-coated culture dishes, increased attachment to ECM was observed for ovarian cancer cells compared with mesothelial cells.[48] In the case of using ovarian cancer spheroids, it has been shown that these use myosin-generated force when breaching through the mesothelial cell monolayer; moreover, Iwanicki *et al.* reported that ovarian cancer spheroids use myosin-generated force to breach and remove the mesothelial cell monolayer.[49] Further, the animal model described here benefits from the use of an immunocompetent host who offers an environment conducive to mesothelial cells, successfully stimulating the migration of white blood cells in response to secreted inflammatory mediators and possibly leading to the increased speed in orthotopic CS-derived tumor development compared with ICS-derived ovarian tumors. In CS-derived tumor-bearing animals, we also observed metastatic lesions throughout the peritoneal cavity, including the diaphragm at only 8 weeks post-transplantation. CS-derived ovarian tumors were breaking through the ovarian capsule at already 4 weeks post-transplantation, possibly facilitating the intraperitoneal tumor spread described earlier (Fig. 6).

Angiogenesis, indirectly documented by immunostaining for VEGF and CD31, was increased in CS compared with ICS tumors. VEGF expression was notably elevated in CS-derived tumors already at 1 week after engraftment. We believe that such VEGF expression in early stages of ovarian tumorigenesis may be an avenue for targeted therapy.[50–52] As reported by Shimizu *et al.*,[28] neovascularization was also detected in cardiac CS grafts at 3 weeks post-transplantation *in vivo*. Sekiya *et al.* reported that pulsatile cardiac CSs contained significant amounts of endothelial cells, and these endothelial cells formed a network-like construct within only 4 days in culture,[53] and demonstrated continuous VEGF expression in these cultured CS *in vitro*. These examples may, in part, explain the difference observed in ovarian volumes and weights in CS-derived compared woth ICS-derived tumors. Microvascular-like formations from the CS to host ovary may have been generated within the first 7 days after transplantation, resulting in improved tumor initiation, growth, invasion, and metastatic potential. In support of this hypothesis, CD31 immunostaining confirmed a significant increase in vessel density in the CS-derived tumors at the 8-week observation time point compared with ICS-derived tumors.

In summary, we have designed and characterized a new, preclinical ovarian cancer animal model utilizing an immunocompetent host and CS technology to form orthotropic, syngeneic allografts with properties that closely replicate human EOC. We have also demonstrated advantages of this model, including the potential benefits directly related to CS technology (intact cell junctions, surface protein and growth factor expression, enhanced angiogenesis, accelerated initiation, growth, invasion, and metastases) as well as the advantages of orthotopic engraftment, which more closely mimics the origin of human cancer. We hypothesize that this model may serve as a more accurate predictor of future clinical efficacy and provide for more economical screening of anticancer drug candidates in the future.

Acknowledgments

The authors thank Yongen Sun, MD, for his expertise and surgical skills in conducting animal experiments. This study was supported by grants from the University of Utah's Department of Obstetrics and Gynecology, the University of Utah Program in Personalized Health Care and Formation of Innovation Center for Fusion of Advanced Technologies in the Special Coordination Funds for Promoting Science and Technology ''Cell Sheet Tissue Engineering Center (CSTEC),'' and the Global Center of Excellence (GCOE) Program, Multidisciplinary Education and Technology and Research Center for Regenerative Medicine (MERCREM), from the Ministry of Education, Culture, Sports Science, and Technology (MEXST), Japan.

Disclosure Statement

Teruo Okano is a founder and director of the board of CellSeed, Inc., licensing technologies and patents from Tokyo Women's Medical University. Teruo Okano is also a shareholder of CellSeed, Inc., Tokyo Women's Medical University and is receiving research funds from CellSeed, Inc.

References

1. Jemal, A., Bray, F., Center, M.M., Ferlay, J., Ward, E., and Forman, D. Global cancer statistics. CA Cancer J Clin **61,** 69, 2011.
2. Bast, R.C., Jr., Hennessy, B., and Mills, G.B. The biology of ovarian cancer: new opportunities for translation. Nat Rev Cancer **9,** 415, 2009.
3. Levanon, K., Crum, C., and Drapkin, R. New insights into the pathogenesis of serous ovarian cancer and its clinical impact. J Clin Oncol **26,** 5284, 2006.
4. Gordon, P.S., and Fishman, D. Early detection of ovarian cancer. In: Liane Deligdisch, Nathan G. Kase, Carmel J. Cohen, eds. Altchek's Diagnosis and Management of Ovarian Disorders, third Edition. Cambridge, United Kingdom: Cambridge University Press, 2013, pp. 357–358.
5. Vang, R., Shih, I.E.M., and Kurman, R.J. Ovarian low-grade and high-grade serous carcinoma: pathogenesis, clinicopathologic and molecular biologic features, and diagnostic problems. Adv Anat Pathol **16,** 267, 2009.
6. Malpica, A., Deavers, M.T., Lu, K., Bodurka, D.C., Atkinson, E.N., Gershenson, D.M., and Silva, E.G. Grading ovarian serous carcinoma using a two-tier system. Am J Surg Pathol **28,** 496, 2004.
7. Landen, C.N., Jr., Birrer, M.J., and Sood, A.K. Early events in the pathogenesis of epithelial ovarian cancer. J Clin Oncol **26,** 995, 2008.
8. Kelland, L.R. Of mice and men: values and liabilities of the athymic nude mouse model in anticancer drug development. Eur J Cancer **40,** 827, 2004.
9. Robert, M.H. Orthotopic metastatic mouse models for anticancer drug discovery and evaluation: a bridge to the clinic. Invest New Drugs **17,** 343, 1999.
10. Krarup, T. Oocyte destruction and ovarian tumorigenesis after direct application of a chemical carcinogen (9:0-dimethyl-1:2-benzanthrene) to the mouse ovary. Int J Cancer **4,** 61, 1969.
11. Jacobs, A.J., Curtis, G.L., Newland, J.R., Wilson, R.B., and Ryan, W.L. Chemical induction of ovarian epithelial carcinoma. Gynecol Oncol **18,** 177, 1984.
12. Tunca, J.C., Ertürk, E., Ertürk, E., and Bryan, G.T. Chemical induction of ovarian tumors in rats. Gynecol Oncol **21,** 54, 1985.
13. Greenaway, J., Moorehead, R., Shaw, P., and Petrik, J. Epithelial-stromal interaction increases cell proliferation, survival and tumorigenicity in a mouse model of human epithelial ovarian cancer. Gynecol Oncol **108,** 385, 2008.
14. Godwin, A.K., Testa, J.R., Handel, L.M., Liu, Z., Vanderveer, L.A., Tracey, P.A., and Hamilton, T.C. Spontaneous transformation of rat ovarian surface epithelial cells: association with cytogenetic changes and implications of repeated ovulation in the etiology of ovarian cancer. J Natl Cancer Inst **84,** 592, 1992.
15. James, E.T., Rakesh, K.S., Isaiah, J.F., and Avraham, R. Murine models to evaluate novel and conventional therapeutics strategies for cancer. AJP **170,** 793, 2007.
16. Shoemaker, R.H. The NCI60 human tumour cell line anticancer drug screen. Nat Rev Cancer **6,** 813, 2006.
17. Alexander, K. What's wrong with our cancer models? Nat Rev **4,** 161, 2005.
18. Yamato, M., Akiyama, Y., Kobayashi, J., Yang, J., Kikuchi, A., and Okano, T. Temperature-responsive cell culture surfaces for regenerative medicine with cell sheet engineering. Prog Polym Sci **32,** 1123, 2007.
19. Yamada, N., Okano, T., Sakai, H., Karikusa, F., Sawasaki, Y., and Sakurai, Y. Thermo-responsive polymeric surfaces; control of attachment and detachment of cultured cells. Makromol Chem Rapid Commun **11,** 571, 1990.
20. Okano, T., Yamada, N., Sakai, H., and Sakurai, Y. A novel recovery system for cultured cells using plasma-treated polystyrene dishes grafted with poly (N-isopropylacrylamide). J Biomed Mater Res **27,** 1243, 1993.
21. Matsuda, N., Shimizu, T., Yamato, M., and Okano, T. Tissue engineering based on cell sheet technology. Adv Mater **19,** 3089, 2007.
22. Ohashi, K., Yokoyama, T., Yamato, M., Kuge, H., Kanehiro, H., Tatsumi, M., Amanuma, T., Iwata, H., Yang, J., Okano, T., and Nakajima, Y. Engineering functional two- and three dimensional liver systems *in vivo* using hepatic tissue sheets. Nat Med **13,** 880, 2007.
23. Shimizu, T., Sekine, H., Isoi, Y., Yamato, M., Kikuchi, A., and Okano, T. Long-term survival and growth of pulsatile myocardial tissue grafts engineered by the layering of cardiomyocyte sheets. Tissue Eng **12,** 499, 2006.
24. Kanzaki, M., Yamato, M., Yang, J., Sekine, H., Takagi, R., Isaka, T., Okano, T., and Onuki, T. Functional closure of visceral pleural defects by autologous tissue engineered cell sheets. Eur J Cardiothorac Surg **34,** 864, 2008.
25. Iwata, T., Yamato, M., Tsuchioka, H., Takagi, R., Mukobata, S., Washio, K., Okano, T., and Ishikawa, I. Periodontal regeneration with multi-layered periodontal ligament-derived cell sheets in a canine model. Biomaterials **30,** 2716, 2009.
26. Sekine, H., Shimizu, T., Dobashi, I., Matsuura, K., Hagiwara, N., Takahashi, M., Kobayashi, E., Yamato, M., and Okano, T. Cardiac cell sheet transplantation improves damaged heart function via superior cell survival in comparison with dissociated cell injection. Tissue Eng Part A **17,** 2973, 2011.
27. Memon, I.A., Sawa, Y., Fukushima, N., Matsumiya, G., Miyagawa, S., Taketani, S., Sakakida, S.K., Kondoh, H., Aleshin, A.N., Shimizu, T., Okano, T., and Matsuda, H. Repair of impaired myocardium by means of implantation of engineered autologous myoblast sheets. J Thorac Cardiovasc Surg **130,** 1333, 2005.

28. Shimizu, T., Yamato, M., Isoi, Y., Akutsu, T., Setomaru, T., Abe, K., Kikuchi, A., Umezu, M., and Okano, T. Fabrication of pulsatile cardiac tissue grafts using a novel 3-dimensional cell sheet manipulation technique and temperatureresponsive cell culture surfaces. Circ Res **90,** e40, 2002.
29. Nishida, K., Yamato, M., Hayashida, Y., Watanabe, K., Yamamoto, K., Adachi, E., Nagai, S., Kikuchi, A., Maeda, N., Watanabe, H., Okano, T., and Tano, Y. Corneal reconstruction with tissue-engineered cell sheets composed of autologous oral mucosal epithelium. N Engl J Med **351,** 1187, 2004.
30. Miyagawa, S., Sawa, Y., Sakakida, S., Taketani, S., Kondoh, H., Memon, I.A., Imanishi, Y., Shimizu, T., Okano, T., and Matsuda, H. Tissue cardiomyoplasty using bioengineered contractile cardiomyocyte sheets to repair damaged myocardium: their integration with recipient myocardium. Transplantation **80,** 1586, 2005.
31. Ohki, T., Yamato, M., Murakami, D., Takagi, R., Yang, J., Namiki, H., Okano, T., and Takasaki, K. Treatment of esophageal ulcerations using endoscopic transplantation of tissueengineered autologous oral mucosal epithelial cell sheets in a canine model. Gut **55,** 1704, 2006.
32. Kanzaki, M., Yamato, M., Yang, J., Sekine, H., Kohno, C., Takagi, R., Hatakeyama, H., Isaka, T., Okano, T., and Okuni, T. Dynamic sealing of lung air leaks by the transplantation of tissue engineered cell sheets. Biomaterials **28,** 4294, 2007.
33. Arauchi, A., Shimizu, T., Yamato, M., Obara, T., and Okano, T. Tissue-engineered thyroid cell sheet rescued hypothyroidism in rat models after receiving total thyroidectomy comparing with nontransplantation models. Tissue Eng Part A **15,** 3943, 2009.
34. Zhang, L., Yang, N., Garcia, J.R., Mohamed, A., Benencia, F., Rubin, S.C., Allman, D., and Coukos, G. Generation of a syngeneic mouse model to study the effects of vascular endothelial growth factor in ovarian carcinoma. Am J Pathol **161,** 2295, 2002.
35. Cho, S., Sun, Y., Soisson, A.P., Dodson, M.K., Peterson, C.M., Jarboe, E.A., Kennedy, A.M., and Janát-Amsbury, M.M. Characterization and evaluation of preclinical suitability of a syngeneic orthotopic mouse ovarian cancer model. Anticancer Res **33,** 3, 2013.
36. Yamato, M., Utsumi, M., Kushida, A., Konno, C., Kikuchi, A., and Okano, T. Thermo-responsive culture dishes allow the intact harvest of multilayered keratinocyte sheets without dispase by reducing temperature. Tissue Eng **7,** 473, 2001.
37. Anton, K., and Glod, J. Targeting the tumor stroma in cancer therapy. Curr Pharm Biotechnol **10,** 185, 2009.
38. Auersperg, N., Wong, A.S., Choi, K.C., Kang, S.K., and Leung, P.C. Ovarian surface epithelium: biology, endocrinology, and pathology. End Rev **22,** 255, 2001.
39. Amadori, D., Sansoni, E., and Amadori, A. Ovarian cancer: natural history and metastatic pattern. Front Biosci **2,** g8, 1997.
40. Lengyel, E. Ovarian cancer development and metastasis. Am J Pathol **177,** 1053, 2010.
41. Gaggioli, C., Hooper, S., Hidalgo-Carcedo, C., Grosse, R., Marshall, J.F., Harrington, K., and Sahai, E. Fibroblast-led collective invasion of carcinoma cells with differing roles for RhoGTPases in leading and following cells. Nat Cell Biol **9,** 1392, 2007.
42. Kalluri, R., and Zeisberg, M. Fibroblasts in cancer. Nat Rev Cancer **6,** 392, 2006.
43. Kraman, M., Bambrough, P.J., Arnold, J.N., Roberts, E.W., Magiera, L., Jones, J.O., Gopinathan, A., Tuveson, D.A., and Fearon, D.T. Suppression of antitumor immunity by stromal cells expressing fibroblast activation protein-alpha. Science **330,** 827, 2010.
44. Togo, S., Polanska, U.M., Horimoto, Y., and Orimo, A. Carcinoma-associated fibroblasts are a promising therapeutic target. Cancers **5,** 149, 2013.
45. Torng, P.L., Mao, T.L., Chan, W.Y., Huang, S.C., and Lin, C.T. Prognostic significance of stromal metalloproteinase-2 in ovarian adenocarcinoma and its relation to carcinoma progression. Gynecol Oncol **92,** 559, 2004.
46. Roy, R., Yang, J., and Moses, M.A. Matrix metalloproteinases as novel biomarkers and potential therapeutic targets in human cancer. J Clin Oncol **27,** 5287, 2009.
47. Kenny, H.A., Krausz, T., Yamada, S.D., and Lengyel, E. Use of a novel 3D culture model to elucidate the role of mesothelial cells, fibroblasts and extra-cellular matrices on adhesion and invasion of ovarian cancer cells. Int J Cancer **121,** 1463, 2007.
48. Niedbala, M.J., Crickard, K., and Bernacki, R.J. Interactions of human ovarian tumor cells with human mesothelial cells grown on extra-cellular matrix. Exp Cell Res **160,** 499, 1985.
49. Iwanicki, M.P., Davidowitz, R.A., Ng, M.R., Besser, A., Muranen, T., Merritt, M., Danuser, G., Ince, T.A., and Brugge, J.S. Ovarian cancer spheroid use myosin-generated force to clear the mesothelium. Cancer Dis **1,** 144, 2011.
50. Paley, P.J., Staskus, K.A., Gebhard, K., Mohanraj, D., Twiggs, L.B., Carson, L.F., and Ramakrishnan, S. Vascular endothelial growth factor expression in early stage ovarian carcinoma. Cancer **80,** 98, 1997.
51. Ang, J.E., and Kaye, S.B. Molecular targeted therapies in the treatment of ovarian cancer. Adv Gene Mol Cell Ther **1,** 68, 2007.
52. Spannuth, W.A., Sood, A.K., and Coleman, R.L. Angiogenesis as a strategic target for ovarian cancer therapy. Nat Clin Pract **5,** 194, 2008.
53. Sekiya, S., Shimizu, T., Yamato, M., Kikuchi, A., and Okano, T. Bioengineered cardiac cell sheet grafts have intrinsic angiogenic potential. Biochem Biophys Res Commun **341,** 573, 2006.

Address correspondence to:
Margit M. Janát-Amsbury, MD, PhD
Division of Gynecologic Oncology
Department of Obstetrics and Gynecology
University of Utah
Salt Lake City, UT 84112

E-mail: margit.janat-amsbury@hsc.utah.edu

Received: January 16, 2014
Accepted: April 11, 2014
Online Publication Date: May 23, 2014